Development of a Continuous Measurement System for Atmospheric O_2/N_2 Ratio Using a Paramagnetic Analyzer and Its Application in Minamitorishima Island, Japan

Shigeyuki Ishidoya[1], Kazuhiro Tsuboi[2], Shohei Murayama[1], Hidekazu Matsueda[2], Nobuyuki Aoki[3], Takuya Shimosaka[3], Hiroaki Kondo[1], and Kazuyuki Saito[4]

[1]*National Institute of Advanced Industrial Science and Technology (AIST), Tsukuba, Japan*
[2]*Meteorological Research Institute, Tsukuba, Japan*
[3]*National Metrology Institute of Japan, National Institute of Advanced Industrial Science and Technology (AIST), Tsukuba, Japan*
[4]*Japan Meteorological Agency, Tokyo, Japan*

Abstract

A continuous measuring system for atmospheric O_2/N_2 ratio was developed employing a paramagnetic oxygen analyzer. Sample air is allowed to flow through a water trap cooled to −80°C, and is introduced into the analyzer at a flow rate of 100 mL min^{-1} by stabilizing the pressure to an order of 10^{-1} Pa. The analytical reproducibility of the O_2/N_2 ratio achieved by the system is about 5 and 3 per meg for 2 and 30 minutes average values, respectively. The O_2/N_2 ratio values obtained by the system are in good agreement with the values obtained by our traditional system using a mass spectrometer. Using our new system, we started measuring the atmospheric O_2/N_2 ratio at Minamitorishima, Japan since December, 2015. Some preliminary results show clearly the O_2/N_2 day-to-day and seasonal variations that are in the opposite phase with the CO_2 concentration.

(**Citation**: Ishidoya, S., K. Tsuboi, S. Murayama, H. Matsueda, N. Aoki, T. Shimosaka, H. Kondo, and K. Saito, 2017: Development of a continuous measurement system for atmospheric O_2/N_2 ratio using a paramagnetic analyzer and its application in Minamitorishima Island, Japan. *SOLA*, **13**, 230−234, doi:10.2151/sola.2017-042.)

1. Introduction

High precision measurements of the atmospheric O_2/N_2 ratio have been carried out since the early 1990s (Keeling and Shertz 1992). Measurement systems using an interferometer (Keeling 1988), a mass spectrometer (Bender et al. 1994), a paramagnetic analyzer (Manning et al. 1999), a gas chromatograph equipped with a thermal conductivity detector (Tohjima 2000), a vacuum ultraviolet absorption analyzer (Stephens et al. 2003) and a fuel cell analyzer (Stephens et al. 2007) have been used. Although global CO_2 budget has been estimated from observed secular trends of O_2/N_2 using discrete air sampling (e.g. Manning and Keeling 2006), continuous observations have proven to be indispensable in applying O_2/N_2 to evaluate regional carbon cycling related to marine biological productions (e.g. Goto et al. 2017) and fossil fuel emissions (e.g. Minejima et al. 2012). To observe the O_2/N_2 ratio continuously, a commercially available fuel cell analyzer (Sable Systems, Oxzilla FC-II) has been widely used in recent studies (e.g. Stephens et al. 2007; Thompson et al. 2009; Goto et al. 2013; Morgan et al. 2015). As summarized in a technical overview (Sable Systems International 2015), a paramagnetic analyzer has an unlimited life span, which is an advantage compared with a fuel cell analyzer that requires replacement of fuel cells nearly every 2 years. However, one disadvantage of paramagnetic analyzer is that its sensitivity to temperature change is significantly higher than that of a fuel cell analyzer. Nevertheless, Manning et al. (1999) were able to develop a continuous O_2/N_2 measurement system using a paramagnetic oxygen sensor (Servomex Company Inc., PM1155) with a precision and time resolution comparable to those of a system using fuel cell analyzer. Therefore, if a commercially available paramagnetic analyzer with a low enough sensitivity to temperature change is available, then it will be useful for the atmospheric O_2/N_2 ratio measurement community.

In this study we present a newly developed continuous system for the atmospheric O_2/N_2 ratio and CO_2 concentration measurements using a paramagnetic analyzer and a non-dispersive infrared analyzer (NDIR), respectively. We also present preliminary observational results of the O_2/N_2 ratio and CO_2 concentration obtained by using the system at Minamitorishima Island (MNM; 24.28°N, 153.98°E), Japan.

2. The measurement system and its performance

2.1 Measurement system and procedure

Figure 1 shows a schematic diagram of the new measurement system. Sample air is taken from an air intake using a diaphragm pump at a flow rate higher than 10 L min^{-1} and introduced into a 1 L stainless-steel buffer to prevent thermally-diffusive fractionation of air molecules at the air intake (Blaine et al. 2006). Then, much of the air is exhausted from the buffer, and the remaining air is allowed to flow into an electric cooling unit (ECU) No.1 at a flow rate of 100 mL min^{-1} by using a mass flow controller MFC1 (HORIBA STEC, SEC-E40). Some of the exhausted air is introduced into ECU No. 2 and used for drying a water trap as well as for developing the reference pressure for a precise differential pressure sensor described below. This air, of which flow rate is controlled by MFC3, is introduced to the inside of the Nafion tube in Perma Pure Dryer before going to one of the Stirling coolers, to exhaust the melted ice in the trap. Meanwhile, the "purge air", whose flow rate is controlled by MFC4, is introduced to the outside of the Nafion tube. Sample air that passes through ECU No.1 is alternatively introduced into one of the water traps (coolers Nos. 1 and 2) in the Stirling cycle refrigerator (TWINBIRD, SC-UE15R). One trap is cooled to −80°C to remove water vapor from the sample air, and the other trap is heated to melt the ice with flowing ambient dried air from the Nafion tube. After passing through the water trap, dried sample air flows into an NDIR (LiCOR, Li-820) and then to a paramagnetic analyzer (Japan Air Liquid, POM-6E). The pressure of sample air is stabilized to an order of 10^{-1} Pa using a flow regulation valve PV1 (HORIBA STEC, PV-1000) and a precise differential pressure sensor PS1 (Setra, MODEL ASL). The reference pressure (~1050 hPa) of the precise differential pressure sensor is made by using an absolute pressure sensor PS2 (Setra, MODEL 270) and a flow regulation

Corresponding author: Shigeyuki Ishidoya, National Institute of Advanced Industrial Science and Technology (AIST), 16-1 Onogawa, Tsukuba, Ibaraki 305-8569, Japan. E-mail: s-ishidoya@aist.go.jp.

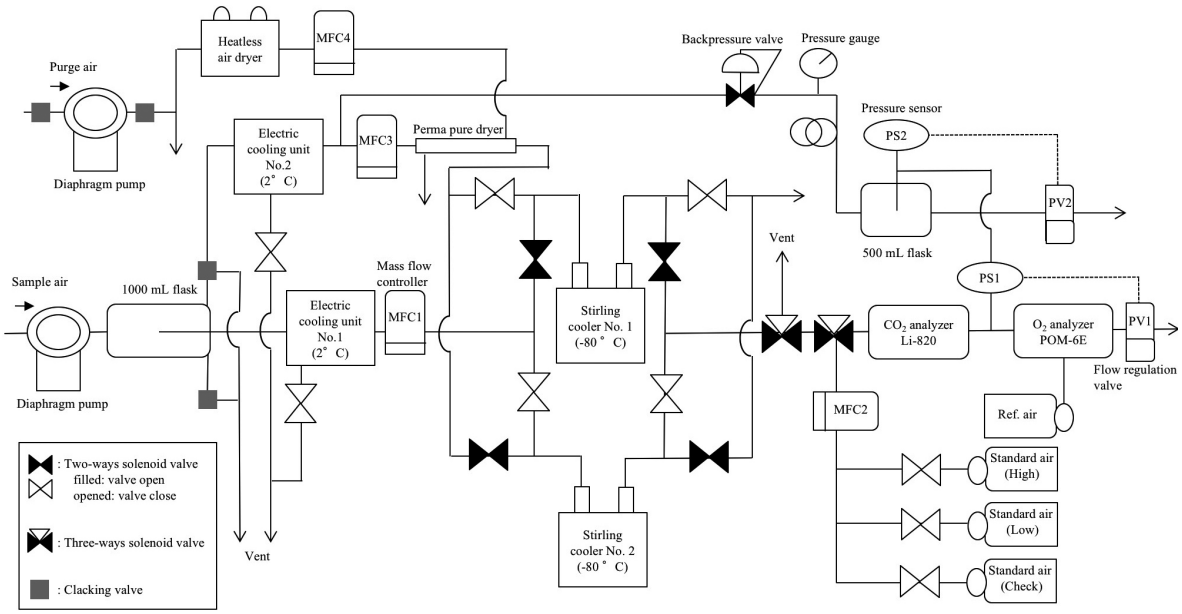

Fig. 1. Schematic diagram of the continuous measurement system for atmospheric $\delta(O_2/N_2)$ and CO_2 concentration.

valve PV2 (HORIBA STEC, PV-1000). An industrially purified air (Japan Fine Products, G1 grade) is used as a reference air for the paramagnetic analyzer. The reference air is introduced into the analyzer at an absolute pressure of 0.4 MPa and the flow rate is adjusted to be about 8 mL min^{-1} by the small orifice in the flow line in the analyzer. High- and low-span standard air were prepared by adding appropriate amounts of pure O_2 or N_2 to industrially prepared CO_2 standard air. To prevent instrumental drift, 5-minute measurements of high and low standard gas are made every 90 minutes of sample air measurements.

The O_2/N_2 ratio is reported in per meg unit:

$$\delta(O_2/N_2) = \left[\frac{(O_2/N_2)_{sample}}{(O_2/N_2)_{standard}} - 1\right] \times 10^6 \quad \text{(eq.1)}$$

where subscripts 'sample' and 'standard' denote the sample air and the standard air, respectively. If O_2 and CO_2 vary in a way that gives the $-O_2$:CO_2 exchange ratio (Oxidative Ratio; OR = $-\Delta O_2 \Delta CO_2^{-1}$ mol mol^{-1}) of 1, then a change of 4.8 per meg of $\delta(O_2/N_2)$ corresponds to 1 μmol mol^{-1} (ppm) changes in O_2. In this study, $\delta(O_2/N_2)$ of each air sample was determined against our primary standard air (Cylinder No. CRC00045) using a mass spectrometer (Thermo Scientific Delta-V) (Ishidoya and Murayama 2014). While the mass spectrometer measures $\delta(O_2/N_2)$ of the sample air directly, the paramagnetic analyzer measures changes in the partial pressure of O_2. Therefore, the paramagnetic analyzer output needs to be expressed as a change in $\delta(O_2/N_2)$. The measurement principle of the paramagnetic analyzer used in this study is detailed in Aoki and Shimosaka (2017). We calculate the sample air $\delta(O_2/N_2)$ from the analyzer output as follows (Manning et al. 1999; Ishidoya et al. 2013):

$$\delta(O_2/N_2) = aV + \frac{\delta X_{CO2}}{(1 - X_{O2})} + \frac{\delta X_{Ar}}{(1 - X_{O2})} \quad \text{(eq.2)}$$

where V is the voltage output from the paramagnetic analyzer, a is the span factor calculated by analyzing the high- and low-span standard gas with known O_2 mole fractions, δX_{CO2} (δX_{Ar}) is the difference in CO_2 (Ar) mole fraction of the sample air from the reference air, in ppm, and X_{O2} is the standard mole fraction of O_2 in dry air. δX_{CO2} and δX_{Ar} account for the respective dilution effects of changes in CO_2 and Ar on the O_2 mole fraction in the fuel cell. By assuming the standard mole fractions of N_2, O_2 and Ar in dry air to be 0.7808, 0.2094 and 0.0093, respectively (Nicolet 1960; Tohjima et al. 2005a), a change of 1 per mil in $\delta(Ar/N_2)$ corresponds to a change of about 9 ppm in δX_{Ar}, leading to a change of 12 per meg in $\delta(O_2/N_2)$. We corrected $\delta(O_2/N_2)$ of the standard gas for the dilution effect using changes in atmospheric Ar, but we did not correct $\delta(O_2/N_2)$ of the sample air for the effect since the variation in atmospheric $\delta(Ar/N_2)$ at the surface is quite small (several tenth per meg) (e.g. Cassar et al. 2008).

2.2 Performance of the measurement system

The performance of the measurement system was evaluated as below. Figure 2 shows typical analytical results for $\delta(O_2/N_2)$ and CO_2 concentration of a standard gas during a 24 hour period. Gray dots and black lines denote 2 and 30 minute running mean values, respectively. Corresponding output signals from the O_2 (paramagnetic) and CO_2 (NDIR) analyzers are also shown. As seen in Fig. 2, the reproducibility mean values of $\delta(O_2/N_2)$ are ±5.0 and ±2.5 per meg while those of CO_2 concentration are ±0.06 and ±0.04 ppm for 2 and 30 minutes, respectively. All the uncertainties reported in this study are expressed as ±1σ. Therefore, we can observe variations in the atmospheric $\delta(O_2/N_2)$ and CO_2 concentration simultaneously by our system with precision and time resolution comparable to those reported by past studies (e.g. Thompson et al. 2009; Morgan et al. 2015).

Figure 3 shows the analytical $\delta(O_2/N_2)$ results of a standard gas for 4.5 days, 2 minute running mean values of the corresponding signal outputs from the paramagnetic analyzer, and the ambient room temperature in our laboratory during the period. With the laboratory temperature controller switched off, the ambient temperature increased gradually with time from 27 to 31°C, with a maximum change rate of 1.4×10^{-4} Ks^{-1}. Although the signal output from the paramagnetic analyzer increased with increasing room temperature, no significant change in the reproducibility of $\delta(O_2/N_2)$ was found, relative to those shown in Fig. 2. However, the temperature sensitivity of the signal output from the paramagnetic analyzer does change depending on the ambient temperature, with a minimum sensitivity achieved at around 20−25°C.

For comparison between the system developed in this study and mass spectrometer (Ishidoya and Murayama 2014), we performed simultaneous measurements using the both methods. Figure 4a shows the values of $\delta(O_2/N_2)$ and CO_2 concentration obtained by the present measurement system (Fig. 1) and by the mass spectrometer at Tsukuba (36°N, 140°E), Japan during July–August, in 2016. Information of the Tsukuba site is detailed in Ishidoya and Murayama (2014). As seen in Fig. 4a, $\delta(O_2/N_2)$

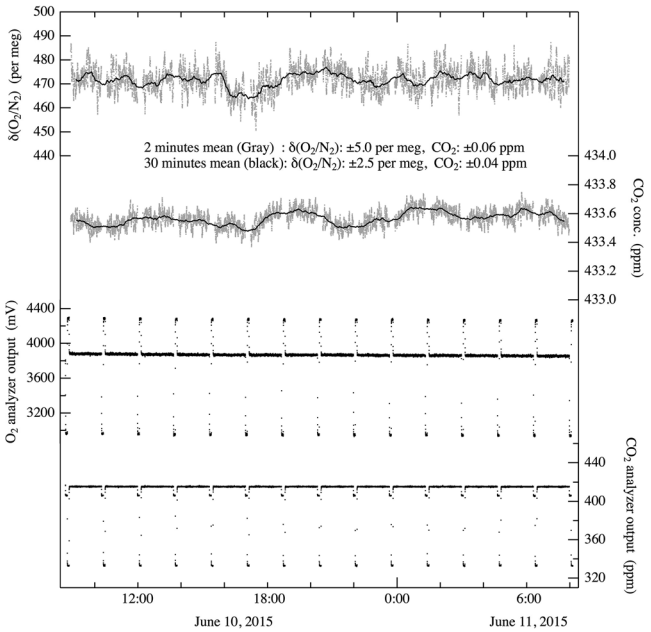

Fig. 2. Typical $\delta(O_2/N_2)$ and CO_2 concentration values of standard gas. Gray dots and black lines denote 2 and 30 minutes running mean values, respectively. Corresponding output signals from the O_2 and CO_2 analyzers are also shown.

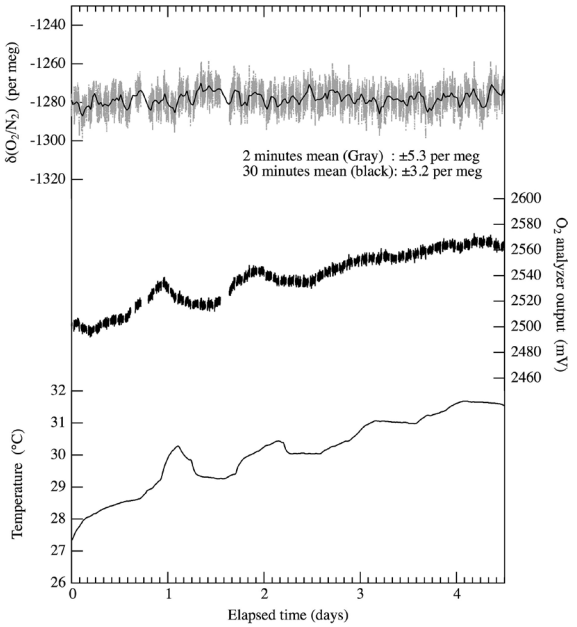

Fig. 3. Typical $\delta(O_2/N_2)$ measurements of standard gas. Corresponding 2 minutes running mean output signals from the O_2 analyzer and the ambient room temperature are also shown.

shows a clear diurnal cycle with a daytime maximum, in opposite phase with CO_2 concentration. Such diurnal cycle is attributable to terrestrial biospheric activities and fossil fuel combustions around Tsukuba, characterized by the decrease and increase of O_2 and CO_2, respectively, in the nighttime stable atmosphere near the surface. Figure 4a also shows that the $\delta(O_2/N_2)$ values observed by the paramagnetic analyzer (hereafter referred to as $\delta(O_2/N_2)_{PA}$) agree well with those obtained by the mass spectrometer (hereafter referred to as $\delta(O_2/N_2)_{MS}$).

Figure 4b shows the relationship between $\delta(O_2/N_2)_{PA}$ and

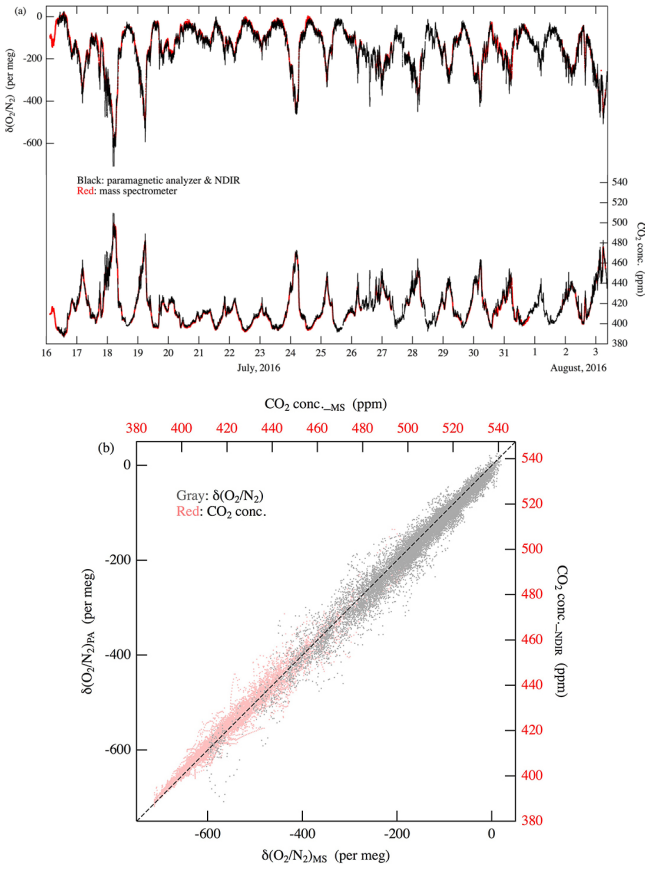

Fig. 4. (a) Observed values of $\delta(O_2/N_2)$ and CO_2 concentration using the paramagnetic analyzer and the NDIR (black) and the mass spectrometer (red) at Tsukuba, Japan for the period 16 July–3 August 2016. (b) Relationship between the $\delta(O_2/N_2)$ values measured by the paramagnetic analyzer ($\delta(O_2/N_2)_{PA}$) and those by the mass spectrometer ($\delta(O_2/N_2)_{MS}$) shown in (a) (gray dots). Dashed line denotes one-to-one relationship between $\delta(O_2/N_2)_{PA}$ and $\delta(O_2/N_2)_{MS}$. Similar relationship but for CO_2 concentration values measured by the NDIR (CO_2 conc._NDIR) and the mass spectrometer (CO_2 conc._MS) are also shown (red dots).

$\delta(O_2/N_2)_{MS}$ shown in Fig. 4a. A linear regression analysis between $\delta(O_2/N_2)_{PA}$ and $\delta(O_2/N_2)_{MS}$ gives a slope of 0.99 with a correlation coefficient of 0.98. However, a standard deviation of $\delta(O_2/N_2)_{PA}$ from the dashed line is ±19 per meg, a value that is larger than those expected from the reproducibility values of measured $\delta(O_2/N_2)_{PA}$ and $\delta(O_2/N_2)_{MS}$ (~ ±5 per meg). This may be due to: (1) the lower flow rate of sample air introduced into the mass spectrometer (10 mL min^{-1}) than in the paramagnetic analyzer, and (2) the larger water trap volume in the inlet system of the mass spectrometer than in the paramagnetic analyzer that could lead to different time responses of the two systems to a rapid change in atmospheric $\delta(O_2/N_2)$. Similar characteristics are also seen in the relationship between the CO_2 concentration values observed by the NDIR (hereafter referred to as CO_2 conc._NDIR) and those by the mass spectrometer (hereafter referred to as CO_2 conc._MS); a linear regression analysis between the CO_2 conc._NDIR and CO_2 conc._MS gives a slope of 0.96 with a correlation coefficient of 0.99, and the standard deviation of CO_2 conc._NDIR from the dashed line is ±2.9 ppm, which is larger than those expected from the reproducibility values of CO_2 conc._NDIR of ±0.05 ppm and CO_2 conc._MS of ±0.3 ppm.

3. Preliminary observational results

We started continuous observations of $\delta(O_2/N_2)$ and CO_2 concentration at the MNM site using the paramagnetic analyzer since

December, 2015. MNM is a small and isolated coral island located 1,850 km southeast of Tokyo, Japan. This site has been operated by the Japan Meteorological Agency (JMA) for the observations of atmospheric trace gases under the Global Atmosphere Watch program of the World Meteorological Organization (WMO/GAW). Information of the MNM site is detailed in Wada et al. (2011).

Figure 5 shows the observed values of $\delta(O_2/N_2)$ and CO_2 concentration at MNM for the period 23 December 2015–17 December 2016. $\delta(O_2/N_2)$ varies in opposite phase from the CO_2 concentration on timescales ranging from interdiurnal variations to seasonal cycles. Peak-to-peak amplitudes of $\delta(O_2/N_2)$ and CO_2 concentration are about 70 per meg and 8 ppm, respectively, which are similar to those observed at Hateruma (24°N, 124°E), Japan located in the same western North Pacific region (e.g. Tohjima et al. 2005b). It is well known that the seasonal and subseasonal variations in the CO_2 concentration are driven mainly by the terrestrial biospheric activities while those in $\delta(O_2/N_2)$ are driven also by the air-sea O_2 flux, since the air-sea CO_2 flux is suppressed by the chemical equilibrium of dissolved inorganic carbon (Keeling et al. 1993). An oxidative ratio OR of 1.1 due to exchange with the terrestrial biosphere (Severinghaus 1995) corresponds to $\delta(O_2/N_2)$: CO_2 concentration ratio of −5.3 per meg ppm^{-1} (-1.1×0.2094^{-1}), where 0.2094 is the mole fraction of atmospheric O_2. Therefore, the deviation of the observed OR from 1.1 can be attributed to the contribution from the air-sea O_2 flux and/or from other sources such as fossil fuel combustion of which average OR is about 1.4 (Keeling 1988).

Figure 6a shows a relationship between the observed values of $\delta(O_2/N_2)$ and CO_2 concentration at MNM. In the figure, OR derived from 1-week average values of $\delta(O_2/N_2)$ and CO_2 concentration gives a value close to 1 and 2 in the summer (June–August) and the winter (December–February), respectively. We also see a significant increase in $\delta(O_2/N_2)$ without an accompanying decrease in the CO_2 concentration during the spring (March–May). These facts suggest that the main contributors to those changes in the 1-week average values of $\delta(O_2/N_2)$ and the CO_2 concentration at MNM are the terrestrial biospheric flux in the summer, both the terrestrial biospheric flux and the air-sea O_2 flux in the winter, and the air-sea O_2 flux only in the spring. The influence of the north-south atmospheric transport on the observed $\delta(O_2/N_2)$ and the CO_2 concentration is also significant at MNM, especially in the winter (discussed below). Therefore, an evaluation of the contribution from the atmospheric transport of fossil fuel combustion is also needed.

In order to examine variations shorter than the seasonal and subseasonal timescales, we show in Fig. 6b the day-to-day variations in $\delta(O_2/N_2)$ and CO_2 concentration (ΔO_2 and ΔCO_2, respectively) in the winter (late December 2015–early March 2016) obtained by subtracting the 1-week average values from the 1-day averages in Fig. 5. Also shown in Fig. 6b are the average latitude locations of the 3.5-day back trajectory origins from MNM calculated using HYSPLIT (Stein et al. 2015; Rolph 2017). As expected, ΔO_2 varies in opposite phase with ΔCO_2. We also note that the negative ΔO_2 values are associated with trajectories from high latitudes. The average OR for the period, derived from a linear regression analysis between the ΔO_2 and ΔCO_2, is 2.0. We also examined the relationship between ΔCO_2 and ΔCO, obtained by applying the same procedure to CO concentration observed continuously by JMA (e.g. Wada et al. 2011), and found that the wintertime average $\Delta CO \Delta CO_2^{-1}$ ratio during the period in Fig. 6b agrees with that expected from fossil fuel combustion (e.g. Niwa et al. 2014). These facts suggest that the wintertime day-to-day variations at MNM are driven by the variations in the north-south

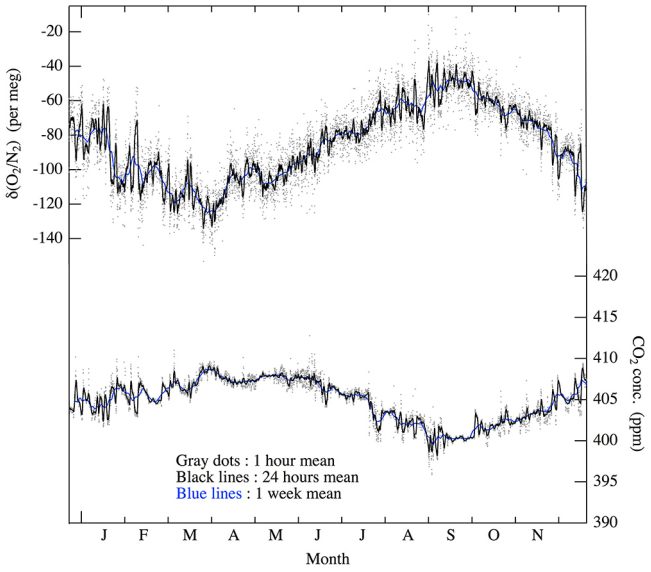

Fig. 5. Observed values of $\delta(O_2/N_2)$ and CO_2 concentration at MNM Japan for the period from late December 2015 to mid December 2016. Dots, black and blue solid lines denote 1-hour, 1-day and 1-week average values, respectively.

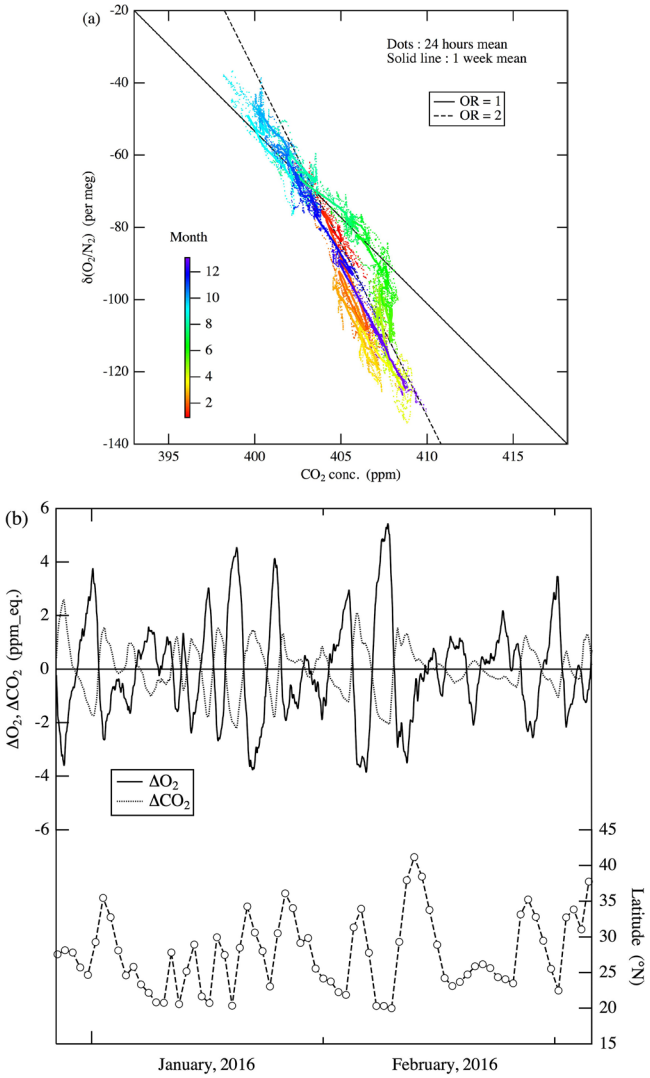

Fig. 6. (a) Relationship between observed values of $\delta(O_2/N_2)$ and CO_2 concentration at MNM shown in Fig. 5. Dots and solid line denote 1-day and 1-week average values, respectively. (b) Day-to-day variations in $\delta(O_2/N_2)$ and CO_2 concentration (ΔO_2 and ΔCO_2) for the period from late December 2015 to early March 2016 obtained by subtracting the 1-week average values from the 1-day averages in (a). Average latitude locations of 3.5-days back trajectory origins from MNM calculated using HYSPLIT are also shown.

atmospheric transport, and that the wintertime latitudinal distributions of $\delta(O_2/N_2)$ and CO_2 concentration are attributed to fossil fuel combustion and air-sea O_2 flux. On the other hand, we also found that the correlation between ΔO_2 and the average latitude of the back trajectory origins are not clear in the spring and summer. This can be interpreted if the high latitude air is less affected by fossil fuel combustion in spring and summer than in winter and/or the local air-sea O_2 flux resulting from marine biological activities around MNM is the dominant cause to drive the ΔO_2 variations in spring and summer. In this regard, Yamagishi et al. (2008) and Goto et al. (2017) discussed the relationships between the short-term variations in $\delta(O_2/N_2)$ observed at northern mid-to-high latitudinal sites and the marine biological activities around the sites. The continuous observation of $\delta(O_2/N_2)$ at MNM will be maintained to evaluate the atmospheric transport processes and the marine biological activities around MNM in more detail.

Acknowledgements

We would like to thank JANS Co. Ltd. for support in designing the measurement system used in this study. Our observation was supported by the members of Minamitorisima Station and Japan Meteorological Agency. This study was partly supported by the JSPS KAKENHI Grant Number 24241008 and 15H02814, and Global Environment Research Account for National Institutes. The authors acknowledge the NOAA Air Resources Laboratory (ARL) for the provision of the HYSPLIT transport and dispersion model and/or READY website (http://www.ready.noaa.gov) used in this publication.

Edited by: D. Zhang

References

Aoki, N., and T. Shimosaka, 2017: Development of an analytical system based on a paramagnetic oxygen analyzer for verification of high precision oxygen standards. *Anal. Sci.*, in review.

Bender, M. L., P. P. Tans, J. T. Ellis, J. Orchard, and K. Habfast, 1994: High precision isotope ratio mass spectrometry method for measuring the O_2/N_2 ratio of air. *Geochim. Cosmochim. Acta*, **58**, 4751−4758.

Blaine, T. W., R. F. Keeling, and W. J. Paplawsky, 2006: An improved inlet for precisely measuring the atmospheric Ar/N_2 ratio. *Atmos. Chem. Phys.*, **6**, 1181−1184.

Cassar, N., G. A. Mckinley, M. L. Bender, R. Mika, and M. Battle, 2008: An improved comparison of atmospheric Ar/N2 time series and paired ocean-atmosphere model predictions. *J. Geophys. Res.*, **113**, D21122, doi:10.1029/2008JD009817.

Goto, D., S. Morimoto, S. Ishidoya, A. Ogi, S. Aoki, S., and T. Nakazawa, 2013: Development of a high precision continuous measurement system for the atmospheric O_2/N_2 ratio and its application at Aobayama, Sendai, Japan. *J. Meteor. Soc. Japan*, **91**, 179−192.

Goto, D., S. Morimoto, S. Aoki, P. K. Patra, and T. Nakazawa, 2017: Seasonal and short-term variations in atmospheric potential oxygen at Ny-Ålesund, Svalbard. *Tellus B*, **69**, 1311767, doi:10.1080/16000889.2017.1311767.

Ishidoya, S., S. Murayama, C. Takamura, H. Kondo, N. Saigusa, D. Goto, S. Morimoto, N. Aoki, S. Aoki, and T. Nakazawa, 2013: O_2:CO_2 exchange ratios observed in a cool temperate deciduous forest ecosystem of central Japan. *Tellus B*, **65**, 21120, doi:10.3402/tellusb.v65i0.21120.

Ishidoya, S., and S. Murayama, 2014: Development of high precision continuous measuring system of the atmospheric O_2/N_2 and Ar/N2 ratios and its application to the observation in Tsukuba, Japan. *Tellus B*, **66**, 22574, doi:10.3402/tellusb.v66.22574.

Keeling, R. F., 1988: Development of an interferometric oxygen analyzer for precise measurement of the atmospheric O_2 mole fraction. PhD thesis, Harvard University, Cambridge.

Keeling, R. F., and S. R. Shertz, 1992: Seasonal and interannual variations in atmospheric oxygen and implications for the global carbon cycle. *Nature*, **358**, 723−727.

Keeling, R. F., M. L. Bender, and P. P. Tans, 1993: What atmospheric oxygen measurements can tell us about the global carbon cycle. *Global Biogeochem. Cy.*, **7**, 37−67.

Manning, A. C., R. F. Keeling, and J. P. Severinghaus, 1999: Precise atmospheric oxygen measurements with a paramagnetic oxygen analyzer. *Global Biogeochem. Cy.*, **13**, 1107−1115.

Manning, A. C., and R. F. Keeling, 2006: Global oceanic and terrestrial biospheric carbon sinks from the Scripps atmospheric oxygen flask sampling network. *Tellus B*, **58**, 95−116.

Minejima, C., M. Kubo, Y. Tohjima, H. Yamagishi, Y. Koyama, S. Maksyutov, K. Kita, and H. Mukai, 2012: Analysis of $\Delta O_2/\Delta CO_2$ ratios for the pollution events observed at Hateruma Island, Japan. *Atmos. Chem. Phys.*, **12**, 2713−2723, doi:10.5194/acp-12-2713-2012.

Morgan, E. J., J. V. Lavrič, T. Seifert, T. Chicoine, A. Day, J. Gomez, R. Logan, J. Sack, T. Shuuya, E. G. Uushona, K. Vincent, U. Schultz, E.-G. Brunke, C. Labuschagne, R. L. Thompson, S. Schmidt, A. C. Manning, and M. Heimann, 2015: Continuous measurements of greenhouse gases and atmospheric oxygen at the Namib Desert atmospheric observatory. *Atmos. Meas. Tech.*, **8**, 2233−2250, doi:10.5194/amt-8-2233-2015, 2015.

Nicolet, M., 1960: The properties and constitution of the upper atmosphere. *Physics of the Upper Atmosphere*, J. A. Ratcliffe, Ed., 17–71, Elsevier, New York.

Niwa, Y., K. Tsuboi, H. Matsueda, Y. Sawa, T. Machida, M. Nakamura, T. Kawasato, K. Saito, S. Takatsuji, K. Tsuji, H. Nishi, K. Dehara, Y. Baba, D. Kuboike, S. Iwatsubo, H. Ohmori, and Y. Hanamiya, 2014: Seasonal variations of CO_2, CH_4, N_2O and CO in the mid-troposphere over the Western North Pacific observed using a C-130H cargo aircraft. *J. Meteor. Soc. Japan*, **92**, doi:10.2151/jmsj.2014-104.

Rolph, G., A. Stein, and B. Stunder, 2017: Real-time Environmental Applications and Display sYstem: READY. *Environ. Model. Software*, **95**, 210−228 (Available online at http://www.ready.noaa.gov, accessed 26 June 2017).

Sable Systems International, 2015: Selecting an O_2 Analyzer for Respirometry, TECHNICAL OVERVIEW. (Available online at https://www.sablesys.com/wp-content/uploads/Sable-Systems-International_White_Paper_O2-Analyzer.pdf, accessed 2 July 2017).

Severinghaus, J., 1995: Studies of the terrestrial O_2 and carbon cycles in sand dune gases and in biosphere 2. Ph. D. thesis, Columbia University, New York.

Stein, A. F., R. R. Draxler, G. D. Rolph, B. J. B. Stunder, M. D. Cohen, and F. Ngan, 2015: NOAA's HYSPLIT atmospheric transport and dispersion modeling system. *Bull. Amer. Meteor. Soc.*, **96**, 2059−2077.

Stephens, B. B., R. F. Keeling, and W. J. Paplawsky, 2003: Shipboard measurements of atmospheric oxygen using a vacuum-ultraviolet absorption technique. *Tellus B*, **55**, 857−878.

Stephens, B. B., P. S. Bakwin, P. P. Tans, R. M. Teclaw, and D. Baumann, 2007: Application of a differential fuel-cell analyzer for measuring atmospheric oxygen variations. *J. Atmos. Oceanic Technol.*, **24**, 82−94.

Thompson, R. L., A. C. Manning, E. Gloor, U. Schultz, T. Seifert, F. Hänsel, A. Jordan, and M. Heimann, 2009: In-situ measurements of oxygen, carbon monoxide and greenhouse gases from Ochsenkopf tall tower in Germany. *Atmos. Meas. Tech.*, **2**, 573−591, doi:10.5194/amt-2-573-2009.

Tohjima, Y., 2000: Method for measuring changes in the atmospheric O_2/N_2 ratio by a gas chromatograph equipped with a thermal conductivity detector. *J. Geophys. Res.*, **105**, 14575−14584.

Tohjima, Y., T. Machida, T. Watai, I. Akama, T. Amari, and Y. Moriwaki, 2005a: Preparation of gravimetric standards for measurements of atmospheric oxygen and re-evaluation of atmospheric oxygen concentration. *J. Geophys. Res.*, **110**, D11302, doi:10.1029/2004JD005595.

Tohjima, Y., H. Mukai, T. Machida, Y. Nojiri, and M. Gloor, 2005b: First measurements of the latitudinal atmospheric O_2 and CO_2 distributions across the western Pacific. *Geophys. Res. Lett.*, **32**, L17805, doi:10.1029/2005GL023311.

Wada, A., H. Matsueda, Y. Sawa, K. Tsuboi, and S. Okubo, 2011: Seasonal variation of enhancement ratios of trace gases observed over 10 years in the western North Pacific. *Atmos. Environ.*, **45**, 2129−2137, doi:10.1016/j.atmosenv.2011.01.043.

Yamagishi, H., Y. Tohjima, H. Mukai, and K. Sasaoka, 2008: Detection of regional scale sea-to-air oxygen emission related to spring bloom near Japan by using in-situ measurements of the atmospheric oxygen/nitrogen ratio. *Atmos. Chem. Phys.*, **8**, 3325−3335.

Manuscript received 11 September 2017, accepted 9 November 2017
SOLA: https://www.jstage.jst.go.jp/browse/sola/